EUROPEAN ORGANIZATION FOR NUCLEAR RESEARCH

CERN-PPE/L3 Note 2131
July 22, 1997

Measurement of the τ Polarisation and the Spin Correlations in $e^+e^- \rightarrow \tau^+\tau^-$

The L3 Collaboration

Abstract

Using data collected with the L3 detector 1994 and 1995 around the Z resonance, the τ polarisation, $\mathcal{P}_\tau$, is measured as a function of the scattering angle using the decays $\tau^- \rightarrow e^-\bar{\nu}_e\nu_\tau$, $\tau^- \rightarrow \mu^-\bar{\nu}_\mu\nu_\tau$, $\tau^- \rightarrow \pi^-\nu_\tau$ and $\tau^- \rightarrow \rho^-\nu_\tau$. Combining the results with our previous measurement using data from 1990-1993 and assuming lepton universality, the neutral current coupling $\mathcal{A}_l = 2a_lv_l/(a_l^2 + v_l^2)$ is determined to be 0.1538 $\pm$ 0.0080 $\pm$ 0.0047. Without this assumption, the couplings of the electron to the Z, $\mathcal{A}_e$, and of the τ to the Z, $\mathcal{A}_\tau$, are measured to be 0.1576 $\pm$ 0.0137 $\pm$ 0.0039 and 0.1520 $\pm$ 0.0096 $\pm$ 0.0064, respectively. The spin correlation parameters $\mathcal{A}_{TT}$ and $\mathcal{A}_{TN}$ are measured from $\tau^+\tau^- \rightarrow e\mu, e\pi, e\rho, \mu\pi, \mu\rho, \pi\pi, \pi\rho$ and $\rho\rho$ ($+n\nu$, where n=2,3,4) with the result $\mathcal{A}_{TT}$= 1.04 $\pm$ 0.26 $\pm$ 0.06 and $\mathcal{A}_{TN}$= 0.36 $\pm$ 0.26 $\pm$ 0.05.

Submitted to *Int. Europhysics Conference on High Energy Physics, Jerusalem, '97*

1 Introduction

In the process $e^+e^- \to Z \to \tau^+\tau^-$, parity is violated both in the production and the decay of the Z giving rise to non-zero polarisation of the τ leptons in the case of unpolarised electron and positron beams. The τ leptons decay inside the detector allowing measurement of their polarisation. The longitudinal τ polarisation, $\mathcal{P}_\tau$, is defined:

$$\mathcal{P}_\tau = \frac{\sigma_+ - \sigma_-}{\sigma_+ + \sigma_-} \tag{1}$$

where σ_+ (σ_-) is the cross section for production of τ^- [1)] with positive (negative) helicity. The dependence of $\mathcal{P}_\tau$ on the scattering angle, $\cos\theta$, is [1]:

$$\mathcal{P}_\tau(\cos\theta) = -\frac{\mathcal{A}_\tau(1+\cos^2\theta) + 2\mathcal{A}_e\cos\theta}{(1+\cos^2\theta) + 2\mathcal{A}_e\mathcal{A}_\tau\cos\theta}. \tag{2}$$

Here θ is the angle between the τ^- and the incoming electron beam directions. The quantities $\mathcal{A}_e$ and $\mathcal{A}_\tau$ depend on the neutral current couplings of the electron and the τ,

$$\mathcal{A}_l = \frac{2\, a_l v_l}{a_l^2 + v_l^2}\ (l = e, \tau) \tag{3}$$

where a_l and v_l are the axial-vector and vector couplings, respectively, of the neutral lepton current. According to Eqn. (2), $\mathcal{A}_e$ and $\mathcal{A}_\tau$ can be determined simultaneously from a measurement of $\mathcal{P}_\tau(\cos\theta)$. $\mathcal{P}_\tau$ can be measured using the energy spectra of the τ decay products [1, 2] under the assumption of pure (V$-$A) structure in the τ decay. The latter is supported by experimental results [3]. Measurements of $\mathcal{A}_e$ and $\mathcal{A}_\tau$ provide independent determinations of the weak mixing angle $sin^2\Theta_W$, test lepton universality in the neutral current, and improve significantly the precision of electroweak parameter fits which also include forward-backward asymmetries and cross sections. Because $\mathcal{A}_e$ and $\mathcal{A}_\tau$ are linear in a_l and v_l, the relative sign is also measured.

In this paper, semileptonic τ decays $\tau^- \to h^-\nu_\tau$ ($h = \pi, K$ or ρ) [2)] and purely leptonic τ decays $\tau^- \to l^-\bar{\nu}_l\nu_\tau$ ($l = e$ or μ) are analysed. Data collected 1994 and 1995 are used. The results are combined with our previous published measurements using data collected in 1991-1993 [4].

Independent information about other polarisation components is obtained from a measurement of spin correlations of both τ's in the final state. Using the τ decay products to define a coordinate system as shown in Fig. 1, the azimuthal angle ω of the incoming beam electron is measured. The angular distribution in ω is sensitive to the transverse-transverse and transverse-normal spin correlations, $\mathcal{A}_{TT}$ and $\mathcal{A}_{TN}$, respectively [5], where transverse denotes the spin component in the collision plane and normal the spin component perpendicular to this plane. The differential cross-section as a function of ω is given by

$$\frac{d\sigma}{d\omega} = K_1 + K_2[\mathcal{A}_{TT}\cos(2\omega) + \mathcal{A}_{TN}\sin(2\omega)]. \tag{4}$$

[1)] Formulae are given for the decay of the τ^-. In the analysis the charge conjugate decays are also used.
[2)] No distinction between charged pions and kaons is made in $\tau^- \to h^-\nu_\tau$ decay.

The quantities K_1 and K_2 contain kinematical terms that depend on the τ decay channels and additional angular dependencies. The spin correlations can be written in terms of the a_τ and v_τ:

$$\mathcal{A}_{TT} = \frac{|a_\tau|^2 - |v_\tau|^2}{|a_\tau|^2 + |v_\tau|^2} \tag{5}$$

$$\mathcal{A}_{TN} = -\frac{2\Im(v_\tau\ a_\tau^*)}{|a_\tau|^2 + |v_\tau|^2}. \tag{6}$$

Measurements of $\mathcal{P}_\tau$ have been performed at low energy machines [6] and at LEP [7]. Spin correlations have recently been measured by other LEP collaborations [8].

2 Data Analysis

The data collected with the L3 detector [9] at LEP in 1994 and 1995 correspond to a total integrated luminosity of 63 pb^{-1} on the Z resonance, 8 pb^{-1} at $\sqrt{s} = M_Z - 2$ GeV and 9 pb^{-1} at $\sqrt{s} = M_Z + 2$ GeV. All data are used for the $\mathcal{P}_\tau$ measurement. The spin correlations are measured using data from 50 pb^{-1} of integrated luminosity collected on the Z resonance in 1994 exploiting the precise tracking information of the L3 microvertex detector [10].

Events of the process $e^+e^- \to \tau^+\tau^-(\gamma)$ are selected by requiring low track multiplicity. Each event is divided into two hemispheres by a plane perpendicular to the event thrust axis. The identification of electrons, muons, pions and rho mesons is performed separately in each hemisphere. Electrons and muons are identified in the barrel part of the detector, which covers $|\cos\theta| < 0.72$ for electrons and $|\cos\theta| < 0.82$ for muons. Hadrons are identified in the endcaps also, extending the coverage to $|\cos\theta| < 0.93$.

For efficiency and background estimates, Monte Carlo events are generated using the programs KORALZ [11] for $e^+ e^- \to \mu^+\mu^-(\gamma)$ and $e^+e^- \to \tau^+\tau^-(\gamma)$, KORALB [12] for $e^+e^- \to \tau^+\tau^-(\gamma)$, BHAGENE [13] for $e^+ e^- \to e^+ e^-(\gamma)$ and DIAG36 [14] for $e^+ e^- \to e^+ e^- f\bar{f}$, where $f\bar{f}$ is $e^+ e^-$, $\mu^+\mu^-$, $\tau^+\tau^-$ or $q\bar{q}$. The events are simulated with the real-detector Monte Carlo [15], which takes into account the effects of energy loss, multiple scattering, showering and time dependent detector inefficiencies due to malfunctioning components, and reconstructed with the standard L3 reconstruction program. The number of Monte Carlo events in each process is about 10 times larger than the data sample.

2.1 Lepton identification

Electron candidates consist of an energy deposition in the electromagnetic calorimeter (BGO) which is electromagnetic in shape and consistent in position and energy with a track in the central tracker. An associated energy deposition in the hadron calorimeter (HCAL) must be consistent with the residual tail of an electromagnetic shower. Muon candidates consist of tracks in the muon spectrometer originating from the interaction point with a minimum-ionizing particle response in the BGO and HCAL. Muons with energies below 2.5 GeV are stopped in the calorimeters. The electron and muon identification efficiencies are estimated from Monte Carlo and shown in Fig. 2 as functions of the normalized particle energy, $x = E_l/E_{beam}$ ($l = e, \mu$), where E_l is the lepton energy and E_{beam} the beam energy. The average values of the identification efficiencies are 82% and 67% for electrons and muons, respectively.

2.2 Hadron identification

The identification of $\tau^- \to \pi^- \nu_\tau$ and $\tau^- \to \rho^- \nu_\tau$ is based on the central tracker and calorimeter information. An algorithm [4] is applied to disentangle overlapping neutral electromagnetic clusters in the vicinity of the impact point of the charged hadron in the BGO. Around the impact point, which is predicted by the central tracker, a hadronic shower whose shape is taken to be energy independent is subtracted from the energy deposition. Remaining local maxima of energy deposition are subject to electromagnetic neutral cluster identification criteria. For accepted electromagnetic neutral clusters, the energies and angles are determined. Two distinct neutral clusters form a π^0 candidate if their invariant mass is within 40 MeV of the π^0 mass. A single neutral cluster forms a π^0 candidate if its energy exceeds 1 GeV. Its transverse energy profile must be consistent with either a single electromagnetic shower or a two photon hypothesis for which the invariant mass is within 50 MeV of the π^0 mass. The calorimetrical energy of the hadron, consisting of the sum of the hadronic energy depositions in the BGO and the HCAL, is then combined with the measurement of the momentum in the central tracker by maximizing the likelihood for these two measurements to originate from a single hadron. The $\tau^- \to \pi^- \nu_\tau$ identification allows no π^0 candidates and no neutral clusters with energy greater than 0.5 GeV. The energy deposition in the BGO and HCAL must be consistent with the measured track momentum.

To identify $\tau^- \to \rho^- \nu_\tau$ decays, exactly one π^0 candidate is required in the hemisphere. The invariant mass of the $(\pi^-\pi^0)$ system must be in the range 0.45 to 1.20 GeV and its energy must be larger than 5 GeV. The efficiency for $\tau^- \to \pi^- \nu_\tau$ and $\tau^- \to \rho^- \nu_\tau$ identification is estimated from Monte Carlo. The dependency on the normalized pion energy, $x = E_\pi/E_{beam}$, in the $\tau^- \to \pi^- \nu_\tau$ decay, is shown in Fig. 3. For the $\tau^- \to \rho^- \nu_\tau$ decay the efficiency is shown in Fig. 4 as function of the $\tau^- \to \rho^- \nu_\tau$ and $\rho^- \to \pi^-\pi^0$ decay angles. The average efficiencies are 66% (64%) and 71% (58%) in the barrel (endcaps) for pions and rhos, respectively.

2.3 Event selection and background rejection

Events with at least one identified τ decay are retained for the measurement of $\mathcal{P}_\tau$. The fraction of misidentified τ decays in each channel is determined using simulated $\mathrm{e^+e^-} \to \tau^+\tau^-(\gamma)$ events. Cosmic muons are rejected by the requirement that tracks originate from the interaction point and that scintillator hits associated with a muon track are within 2 ns of the beam crossing time. An unidentified hemisphere must be inconsistent with a high energy electron or muon.

Taking the spectral shape of Bhabha and dimuon backgrounds from data and the two photon background shapes from Monte Carlo, the amounts of these backgrounds are estimated from a fit to the data sample itself or to a control data sample.

For the measurement of spin correlations, only events with both τ decays identified as eμ, eπ, eρ, $\mu\pi$, $\mu\rho$, $\pi\pi$, $\pi\rho$ and $\rho\rho$ are used. The final state where both τ's decay into electrons or muons is not used because of high background from $\mathrm{Z} \to \mathrm{e^+\,e^-}(\gamma)$ or $\mathrm{Z} \to \mu^+\mu^-(\gamma)$, respectively. Remaining non-τ background, mainly from radiative dilepton and two photon events, is further reduced by applying the following criteria: The acollinearity angle, ϵ, must satisfy $1^0 < \epsilon < 15^0$ and the transverse momentum of at least one track must be larger than 3 GeV/c. Furthermore, the muon momentum in $\pi\mu$ and $\rho\mu$ final states must be less than $0.8E_{beam}$ and the energy deposit in the BGO is required to be less than $0.35\sqrt{s}$, $0.65\sqrt{s}$ and $0.9\sqrt{s}$ for $\pi\pi$, eπ and $\rho\rho$ final states, respectively.

The number of selected events in each final state, the selection efficiency and the background fractions are given in Table 1 for the final states used in the $\mathcal{P}_\tau$ measurement and in Table 2 for the final states used in the measurement of spin correlations.

Channel	Events	ε (%) in 4π	Bkg. (%) τ	non-τ
e X	16828	45	1.6	3.6
μ X	14452	40	0.9	4.7
π X	12432	42	9.5	3.6
ρ X	23246	38	10.8	1.0
Total	66958			

Table 1: The numbers of selected events, the selection efficiencies and the fractions from τ and non-τ backgrounds for the channels used to measure $\mathcal{P}_\tau$.

Channel	Events	ε (%) in 4π	Bkg. (%) τ	non-τ
e μ	1181	32	2.2	0.2
e π	574	23	9.4	1.2
e ρ	1560	25	13.6	0.1
μ π	717	26	9.5	2.8
μ ρ	1319	23	13.1	0.2
π π	260	23	16.8	0.3
π ρ	1020	21	20.1	0.0
ρ ρ	793	18	22.6	0.0
Total	7424			

Table 2: The numbers of selected events, the selection efficiencies and the fractions from τ and non-τ backgrounds for final states used in the measurement of spin correlations.

3 Methods of the measurements

3.1 Polarisation

Two methods are employed to measure the longitudinal polarisation $\mathcal{P}_\tau$. The first uses expectations for the charged particle spectra in each τ decay channel generated by the Monte Carlo program KORALZ [11] for positive and negative τ^- helicity. KORALZ generates $e^+e^- \to \tau^+\tau^-(\gamma)$ events including the effects of initial state, final state and decay radiation and contributions from γ exchange and (γ-Z) interference. The obtained spectra for the two helicity states after realistic detector simulation and reconstruction are fitted to the data distributions. A binned maximum likelihood method accounting for finite statistics both in data and Monte Carlo [16] is used for the fit. From the relative portion of the two distributions, ${\mathcal{P}_\tau}^{raw}$ is obtained which still contains contributions from QED bremsstrahlung, γ exchange and (γ-Z) interference.

The correlations between two identified τ decays in an event is taken into account when combining results of the individual decay channels.

For the electron and muon spectra, the normalization of the Bhabha and dimuon background is left free in the fit, whereas the two photon and cosmics contributions are fixed to the estimated amounts. The non-τ background is fixed in hadron spectra. The background from other τ decays is also subdivided in two distributions with positive and negative helicity. The relative portion is varied in the fit in correspondence with the signal distributions.

The second method uses analytic formulae for the charged particle spectra for each helicity state including radiative corrections [17]. These spectra are then convoluted with the detector resolution functions and acceptances for each τ decay channel. The resulting spectra are fitted to the background subtracted data.

${\mathcal{P}_\tau}^{raw}$ is measured in nine $\cos\theta$ intervals. The angle θ is approximated by the polar angle of the thrust axis of the event in the τ^- jet direction. The charge determination is ambigous for 0.6 % of the events in the barrel and 2% in the endcaps. A correction applied to each $\cos\theta$ interval accounts for this effect.

The values obtained for ${\mathcal{P}_\tau}^{raw}$ are corrected for QED Bremsstrahlung, γ exchange and (γ-Z) interference contributions, in order to get $\mathcal{P}_\tau$ as given in Eqn.(2), using the program ZFITTER [18]. These corrections, albeit small at the Z, reach the level of a few per cent for off-peak data and partially cancel when averaging measurements from data of nearly equal luminosity below and above the Z peak.

3.2 Spin Correlations

The transverse spin correlations, $\mathcal{A}_{TT}$ and $\mathcal{A}_{TN}$, are obtained from the distribution of the azimuthal angle of the incoming electron, ω, given in Eqn.(4). Two asymmetries, A_{cos} and A_{sin}, are defined in terms of the angle ω:

$$A_{cos} \equiv \frac{\int_{\cos 2\omega>0} d\sigma - \int_{\cos 2\omega<0} d\sigma}{\int_{\cos 2\omega>0} d\sigma + \int_{\cos 2\omega<0} d\sigma} \tag{7}$$

$$A_{sin} \equiv \frac{\int_{\sin 2\omega>0} d\sigma - \int_{\sin 2\omega<0} d\sigma}{\int_{\sin 2\omega>0} d\sigma + \int_{\sin 2\omega<0} d\sigma}. \tag{8}$$

The quantities A_{cos} and A_{sin} are related to the spin correlations,

$$\mathcal{A}_{TT} = \frac{A_{cos}\pi}{2G\tilde{Q}_3}(\tilde{Q}_1 - \mathcal{P}_\tau \tilde{Q}_2) \tag{9}$$

$$\mathcal{A}_{TN} = \frac{A_{sin}\pi}{2G\tilde{Q}_3}(\tilde{Q}_1 - \mathcal{P}_\tau \tilde{Q}_2) \tag{10}$$

where the geometrical factor G is introduced taking into account the fiducial volume cut in $\cos\theta$:

$$G = \frac{(3 - |\cos\theta|^2)}{(3 + |\cos\theta|^2)} \tag{11}$$

and the $\tilde{Q}_i$ functions are given by:

$$\tilde{Q}_i = \int_{\epsilon_1}^{\epsilon_2} Q_i(\epsilon) d\epsilon \quad i = 1, 2, 3. \tag{12}$$

The quantities ϵ_1 and ϵ_2 define the acollinearity angle interval where the measurement is performed. The functions $Q_i(\epsilon)$ are introduced in [5]. The integrals $\tilde{Q}_i$ are calculated numerically following [19] taking into account the masses of the τ decay products. The dependence on $\mathcal{P}_\tau$ in Eqns.(9) and (10) is suppressed because $\tilde{Q}_2$ is a very small quantity after intregration over the ϵ range $1^0 < \epsilon < 15^0$. The background from other τ decays and from non-τ final states is subtracted and an acceptance correction is applied bin by bin. A_{cos} and A_{sin} are computed for each channel separately. Radiative corrections are treated as suggested in [20]. $\mathcal{A}_{TT}$ and $\mathcal{A}_{TN}$, as obtained from Eqns.(9) and (10), are averaged for each exclusive final state.

4 Systematic Errors

4.1 Polarisation

The main sources of systematic errors are the energy scales of the different subdetectors, uncertainties in the background estimations, and biases due to the event selection. The effect of the scale uncertainties is investigated using a fast Monte Carlo simulation with very high statistics which includes the subdetector resolutions and acceptances. The scale uncertainties of the BGO and muon spectrometer are estimated by comparing the detector responses for Bhabha and dimuon data with the beam energy. The central tracker momentum scale uncertainty is determined comparing its momentum measurement with the muon spectrometer result. At low energy, a cross calibration of the central tracker with the BGO and the muon spectrometer is performed using electrons and muons from τ decays and two photon events. The π^0 peak position in the invariant mass $\mathrm{M}(\gamma\gamma)$ is used as an additional constraint. The BGO and the muon spectrometer scale uncertainties are estimated to be 0.5% at low energy and 0.05 % at high energy. The scale ancertainties are interpolated linearly for intermediate energies. This procedure is checked using radiative Bhabha and dimuon events. The momentum scale of the central tracker is verified to 0.5% from 1 to 45 GeV/c. The HCAL scale is estimated at low energy by a comparison with the central tracker momentum measurement and at high energy by the position of the rho resonance in the $(\pi^-\pi^0)$ invariant mass distribution. The scale uncertainty is estimated to be 1% (3%) in the barrel (endcap) and independent of the hadron energy. The responses of the individual subdetectors are varied according to their scale uncertainties. The systematic error on $\mathcal{P}_\tau$ from each source is determined independently and then summed quadratically.

The non-τ background, determined from data distributions as described in section 2.3, is varied within the statistical error of the fit. The corresponding change of $\mathcal{P}_\tau$ is assigned as the systematic error. The systematic error due to background from other τ decays is estimated by varying the branching fractions of the contributing decay channels within their errors [21]. The systematic error due to the selection procedure is estimated by varying the important cuts. The systematic error due to wrong charge measurement is negligible. The theory error accounts for uncertainties in the a_1 modeling in $\tau^- \to a_1^- \nu_\tau$ decays which contribute to the background in the $\tau^- \to \rho^- \nu_\tau$ channel and from the uncertainty in the structure dependent radiation [22] which affects mainly the $\tau^- \to \pi^- \nu_\tau$ channel.

The systematic errors on $\mathcal{P}_\tau$ from each of this sources are given in Tables 4 and 5.

4.2 Spin correlations

Uncertainties in the background from radiative dilepton and two photon final states are critical. These final states fake an asymmetry by exhibiting peaks at 0°/360° and 180° in the ω distribution. This background is estimated for the hadron-lepton final states from control data spectra. For all other final states, the Monte Carlo estimation is used. The background contribution was varied by 50% to estimate the systematic uncertainty. The background from other τ decays is subtracted from the selected data sample using background spectra in ω obtained from KORALB [12] and KORALZ [11] Monte Carlo samples. The choice of the Monte Carlo program has no effect on the measurement. The uncertainty in the τ background contribution is investigated twofold. First, the normalisation is changed by 2%; the effect on $\mathcal{A}_{TT}$ and $\mathcal{A}_{TN}$ is negligible. Second, the background composition is altered by varying the amount of each single τ decay mode by 10%. The systematic error from the detector resolution is investigated by varying the resolution functions within the constraints given by their comparison with $e^+ e^- \to \mu^+\mu^-$ and $e^+ e^- \to e^+ e^-$ control data samples. The error due to $\mathcal{P}_\tau$ in Eqn.(9) and (10) is negligible. The selection cuts of the exclusive final states were changed within reasonable limits. For the radiative corrections an uncertainty of 50% of the correction is assumed. The systematic error contributions are summarized in Table 3.

source	ΔA_{TT}	ΔA_{TN}
background	0.02	0.02
detector resolution	0.04	0.03
radiative corrections	0.02	—
selection	0.03	0.03
total	0.06	0.05

Table 3: The contributions to the systematic errors on $\mathcal{A}_{TT}$ and $\mathcal{A}_{TN}$.

5 Results

5.1 τ Polarisation

Using data from 1994 and 1995, the spectra of the charged decay products for the channels $\tau^- \to e^-\bar{\nu}_e\nu_\tau$, $\tau^- \to \mu^-\bar{\nu}_\mu\nu_\tau$ and $\tau^- \to \pi^-\nu_\tau$, integrated over $\cos\theta$ are shown in Figs. 5 and 6, respectively. The angular distributions for the decays $\tau^- \to \rho^-\nu_\tau$ and $\rho^- \to \pi^-\pi^0$ are shown in Fig. 7. The spectra obtained from the fit with the first method agree well with the data. The measured values for $\mathcal{P}_\tau$, averaged over $\cos\theta$, are given in Table 4. These results are in agreement

channel	$\mathcal{P}_\tau$	stat.	calibration	background	selection	theory
$\tau^- \to e^-\bar{\nu}_e\nu_\tau$	-0.168	0.039	0.009	0.009	0.007	-
$\tau^- \to \mu^-\bar{\nu}_\mu\nu_\tau$	-0.111	0.045	0.009	0.012	0.005	-
$\tau^- \to \pi^-\nu_\tau$	-0.135	0.021	0.016	0.004	0.005	0.002
$\tau^- \to \rho^-\nu_\tau$	-0.168	0.017	0.008	0.003	0.006	-

Table 4: The polarisation $\mathcal{P}_\tau$ averaged over $\cos\theta$ for each decay channel with the statistical and systematic errors.

with the ones obtained using the analytical expressions in the fit. Table 5 lists $\mathcal{P}_\tau$ averaged over the decay channels in each $\cos\theta$ interval along with the statistical and systematic errors. These results combined with our previous measurement using data from 1990-1993 is listed in Table 6 and shown in Fig. 8. From this distribution $\mathcal{A}_e$ and $\mathcal{A}_\tau$ are determined to be:

$\cos\theta$	$\mathcal{P}_\tau$	stat.	MC stat.	calibration	background	selection	theory
-0.93 -0.72	-0.066	0.091	0.030	0.030	0.012	0.010	0.001
-0.72 -0.55	-0.040	0.036	0.011	0.008	0.003	0.004	0.001
-0.55 -0.35	0.028	0.035	0.011	0.008	0.003	0.004	0.001
-0.35 -0.12	-0.082	0.038	0.011	0.007	0.003	0.005	0.001
-0.12 0.12	-0.203	0.036	0.011	0.009	0.003	0.005	0.001
0.12 0.35	-0.247	0.037	0.011	0.008	0.003	0.005	0.001
0.35 0.55	-0.289	0.034	0.010	0.008	0.003	0.004	0.001
0.55 0.72	-0.276	0.036	0.011	0.007	0.003	0.004	0.001
0.72 0.93	-0.260	0.080	0.027	0.027	0.012	0.010	0.001

Table 5: $\mathcal{P}_\tau$, corrected for QED Bremsstrahlung, γ exchange and (γ-Z) interference, as function of $\cos\theta$ from 1994 and 1995 data with the statistical and systematic errors.

$\cos\theta$	$\mathcal{P}_\tau$	stat.	MC stat.	calibration	background	selection	theory
-0.93 -0.72	-0.024	0.051	0.021	0.019	0.009	0.010	0.001
-0.72 -0.55	-0.044	0.027	0.009	0.007	0.002	0.004	0.001
-0.55 -0.35	0.014	0.026	0.008	0.007	0.002	0.004	0.001
-0.35 -0.12	-0.081	0.027	0.009	0.006	0.002	0.005	0.001
-0.12 0.12	-0.155	0.025	0.009	0.007	0.002	0.005	0.001
0.12 0.35	-0.223	0.027	0.009	0.007	0.002	0.005	0.001
0.35 0.55	-0.296	0.025	0.008	0.007	0.002	0.004	0.001
0.55 0.72	-0.273	0.026	0.009	0.006	0.002	0.004	0.001
0.72 0.93	-0.260	0.046	0.019	0.018	0.009	0.010	0.001

Table 6: $\mathcal{P}_\tau$, corrected for QED Bremsstrahlung, γ exchange and (γ-Z) interference, as function of $\cos\theta$ from data collected 1990-1995 with the statistical and systematic errors.

$$
\begin{aligned}
\mathcal{A}_e &= 0.1576 \pm 0.0137(stat.) \pm 0.0039(sys.) \\
\mathcal{A}_\tau &= 0.1520 \pm 0.0096(stat.) \pm 0.0064(sys.)
\end{aligned}
$$

Assuming lepton universality, these results are combined to:

$$\mathcal{A}_l = 0.1538 \pm 0.0080(stat.) \pm 0.0047(sys.).$$

The ratios of the vector to the axial-vector couplings are 0.0793 ± 0.0073 and 0.0764 ± 0.0059 for electrons and taus, respectively. The corresponding values for the weak mixing angle, $sin^2\Theta_W$, are 0.2302 ± 0.0018 and 0.2309 ± 0.0014.

5.2 Results on Spin Correlations

The results obtained for $\mathcal{A}_{TT}$ and $\mathcal{A}_{TN}$ in the individual channels are shown in Fig. 9. The average values for $\mathcal{A}_{TT}$ and $\mathcal{A}_{TN}$ are measured to be:

$$
\begin{aligned}
\mathcal{A}_{TT} &= 1.04 \pm 0.26(stat.) \pm 0.06(sys.) \\
\mathcal{A}_{TN} &= 0.36 \pm 0.26(stat.) \pm 0.05(sys.).
\end{aligned}
$$

The final spectra are shown in Fig. 10.

Since $\mathcal{A}_{TT}$ is not symmetric under the interchange $a_\tau \leftrightarrow v_\tau$, the measured value of $\mathcal{A}_{TT}$ indicates that the weak neutral current interaction is dominated by the axial-vector coupling. In combination with the $\mathcal{A}_\tau$ measurement, the $\mathcal{A}_{TN}$ result can be interpreted as the phase difference between the vector and axial-vector couplings:

$$\tan(\Phi_{v_\tau} - \Phi_{a_\tau}) = -2.5 \pm 1.7 \tag{13}$$

The result has been corrected for the small (γ-Z) interference contribution as given in [5].

6 Acknowledgments

We wish to express our gratitude to the CERN accelerator divisions for the excellent performance of the LEP machine. We acknowledge the contributions of all the engineers and technicians who have participated in the construction and maintenance of this experiment.

References

[1] S. Jadach, Z. Was *et al.*, in 'Z Physics at LEP 1', CERN Report CERN 89-08, eds. G. Altarelli, R. Kleiss and C. Verzegnassi (CERN, Geneva, 1989) Vol. 11, p. 235 and references therein.

[2] K. Hagiwara, A. D. Martin, D. Zeppenfeld, Phys. Lett. **B 235** (1990) 198;
A. Rouge, Z. Phys. **C 48** (1990) 75.

[3] ARGUS Collab., H. Albrecht *et al.*, Phys. Lett. **B 349** (1995) 576;
ALEPH Collab., D. Buskulic *et al.*, Phys. Lett. **B 346** (1995) 379;
L3 Collab., M. Acciari *et al.*, Phys. Lett. **B 377** (1996) 313;
CLEO Collab., J. P. Alexander *et al.*, CLNS 97/1480, CLEO 97-9 (1997).

[4] L3 Collab., M. Acciarri *et al.*, Phys. Lett. **B 341** (1994) 245.

[5] J. Bernabeu *et al.*, Phys. Lett. **B 257** (1991) 219.

[6] W. T. Ford *et al.*, Phys. Rev. **D 36** (1987) 1971;
CELLO Collab.,H. J. Behrend *et al.*, Phys. Lett. **B 127** (1983) 270;
AMY Collab., M. H. Lee *et al.*, KEK preprint **90-70** (1990).

[7] DELPHI Collab., P. Abreu *et al.*, Z. Phys. **C 55** (1992) 555;
ALEPH Collab., D. Buskulic *et al.*, Z. Phys. **C 69** (1996);
OPAL Collab., G. Alexander *et al.*, Z. Phys. **C 72** (1996) 365.

[8] ALEPH Collab., R. Barate *et al.*, CERN-PPE/97-047 (1997);
DELPHI Collab., P. Abreu *et al.*, CERN-PPE/97-034 (1997).

[9] L3 Collab., B. Adeva *et al.*, Nucl. Inst. and Meth. **A 289** (1990) 35;
O. Adriani *et al.*, Nucl. Inst. and Meth. **A 302** (1991) 53;
K. Deiters *et al.*, Nucl. Inst. and Meth. **A 323** (1992) 162.

[10] M. Acciarri *et al.*, Nucl. Inst. and Meth. **A 351** (1994) 300.

[11] S. Jadach, B. F. L. Ward and Z. Was, Comp. Phys. Comm. **79** (1994) 503.

[12] S. Jadach and Z. Was, CERN-TH-7272/94 (1994).

[13] J. H. Field, Phys. Lett. **B 323** (1994) 432;
J. H. Field and T. Riemann, Comp. Phys. Comm **94** (1996) 53.

[14] F. A. Berends, P. H. Daverfeldt and R. Kleiss, Nucl. Phys. **B 253** (1985) 441.

[15] The L3 detector simulation is based on GEANT Version 3.15.
See R. Brun *et al.*, "GEANT 3", CERN DD/EE/84-1 (Revised), September 1987.
The GHEISHA program (H. Fesefeldt, RWTH Aachen Report PITHA 85/02 (1985)) is used to simulate hadronic interactions..

[16] R. Barlow and C. Beeston, Comp. Phys. Comm. **77** (1993) 219.

[17] P. García–Abia, Informes Tecnicos del CIEMAT **783** (1996) 1.

[18] D. Bardin *et al.*, FORTRAN package ZFITTER, and preprint CERN–TH. 6443/92;
D. Bardin *et al.*, Z. Phys. **C 44** (1989) 493;
D. Bardin *et al.*, Nucl. Phys. **B 351** (1991) 1;
D. Bardin *et al.*, Phys. Lett. **B 255** (1991) 290..

[19] F. Sánchez, Phys. Lett. **B 384** (1996) 277.

[20] F. Sánchez, Z. Was, Phys. Lett. **B 351** (1995) 562.

[21] Particle Data Group, Phys. Rev. **D 54** (1996).

[22] M. Finkemeier, Ph.D. Thesis, University of Karlsruhe (1994).

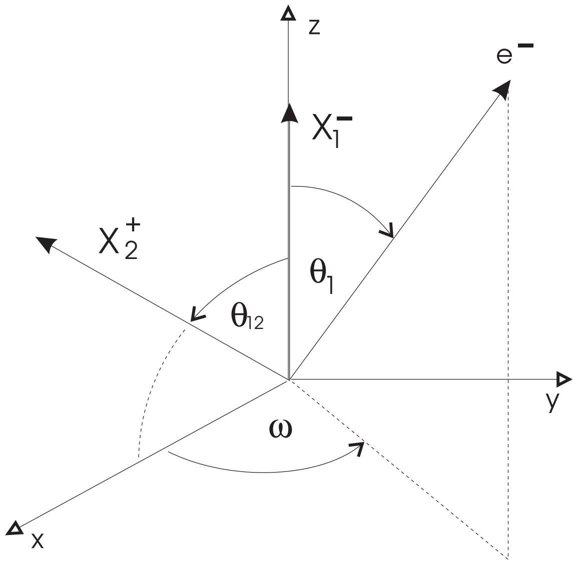

Figure 1: The coordinate system illustrates the definition of the angle ω. X^- and X^+ denote the momenta of the charged decay products of the τ^- and τ^+, respectively.

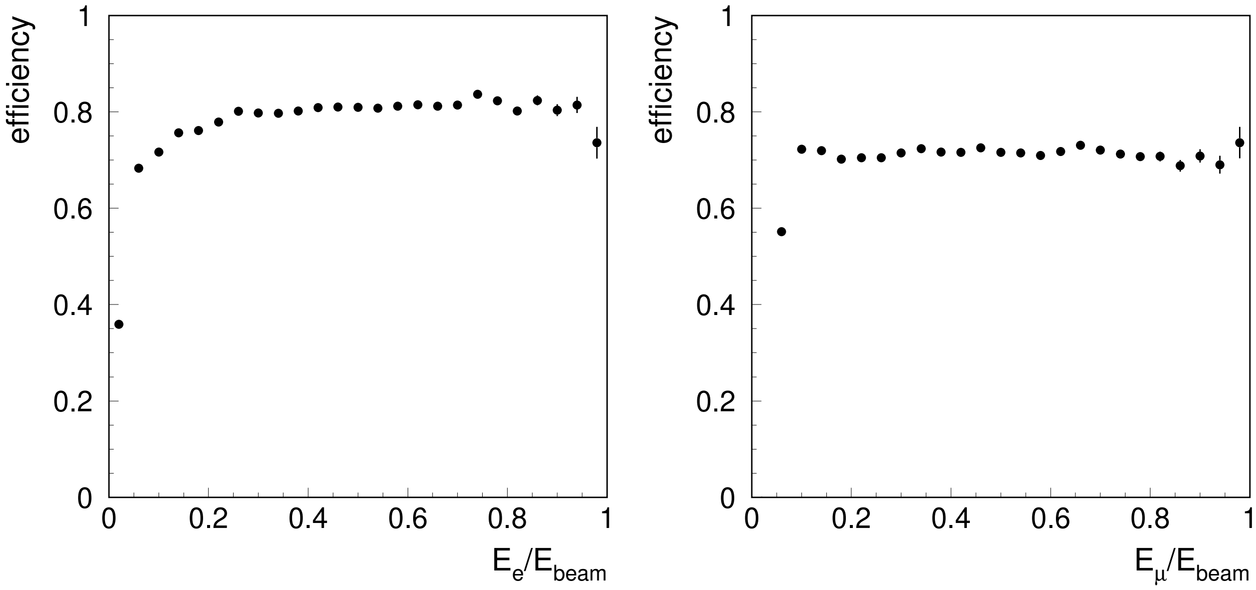

Figure 2: The identification efficiencies for electrons and muons as a function of the normalized energy.

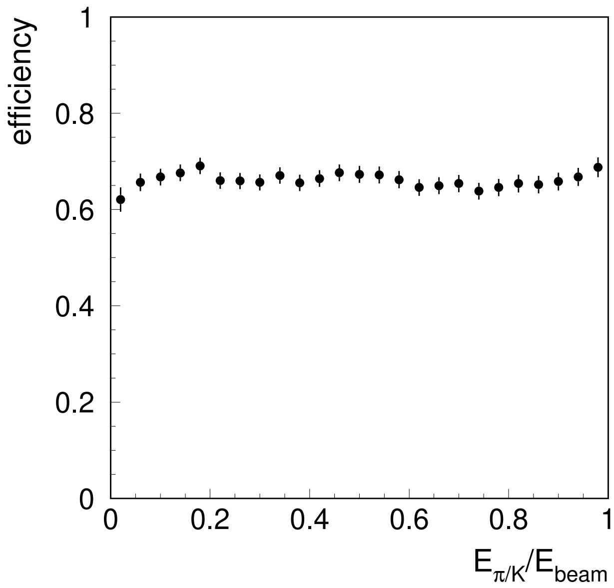

Figure 3: The identification efficiency for pions as a function of the normalized energy.

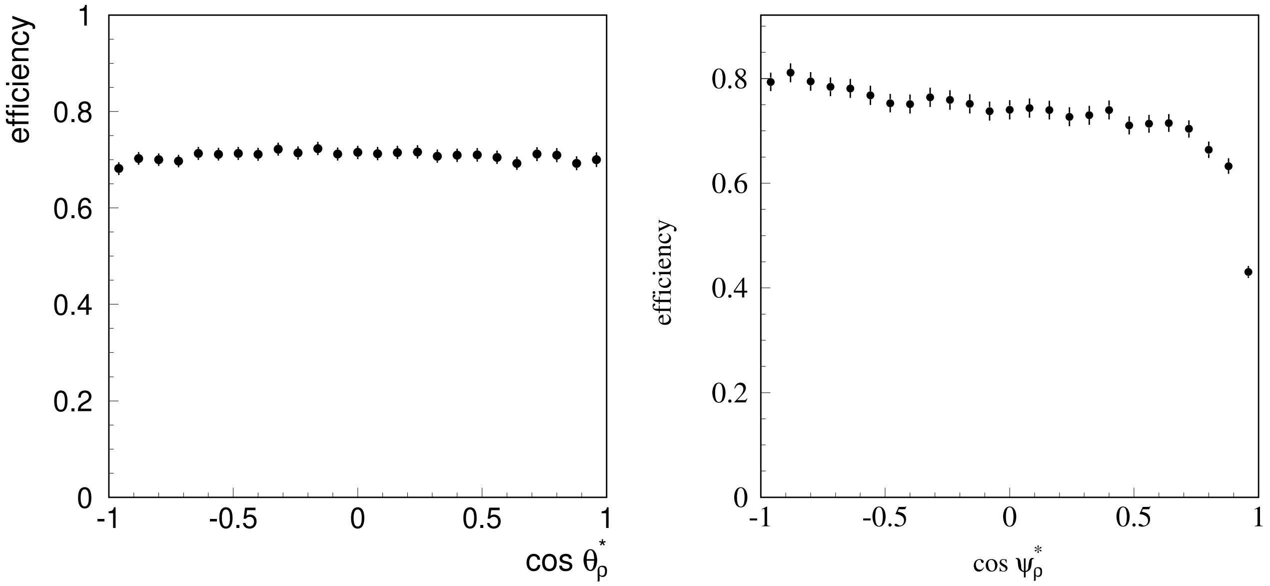

Figure 4: The identification efficiency for rho mesons as a function of the rho polar angle, $\cos\theta^*_\rho$, in the τ rest frame and of the π^- polar angle, $\cos\psi^*_\rho$, in the rho meson rest frame.

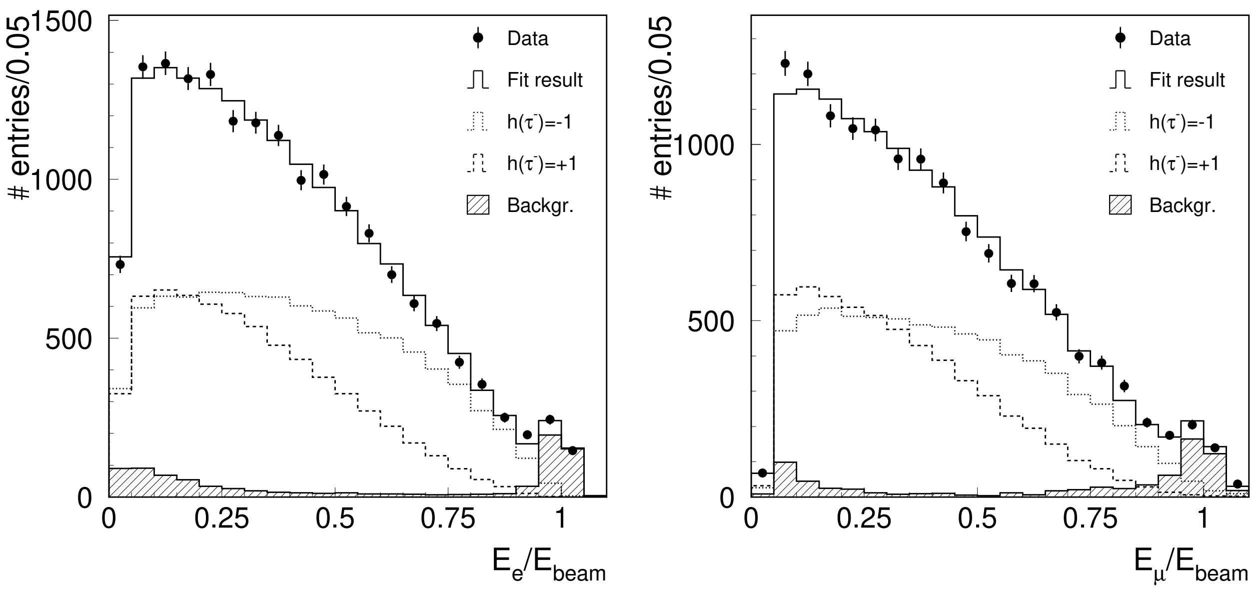

Figure 5: The electron and muon spectra with the results of the fit superimposed.

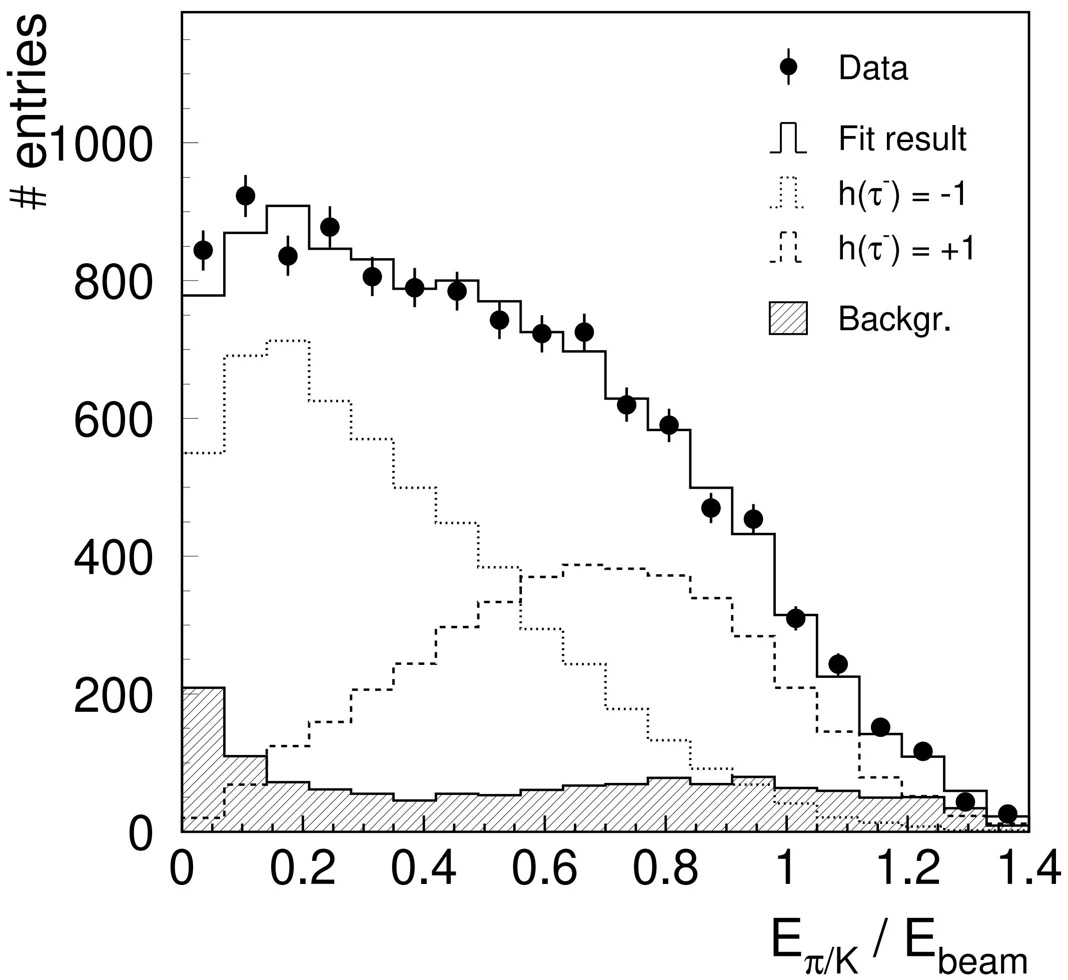

Figure 6: The pion spectrum with the result of the fit superimposed.

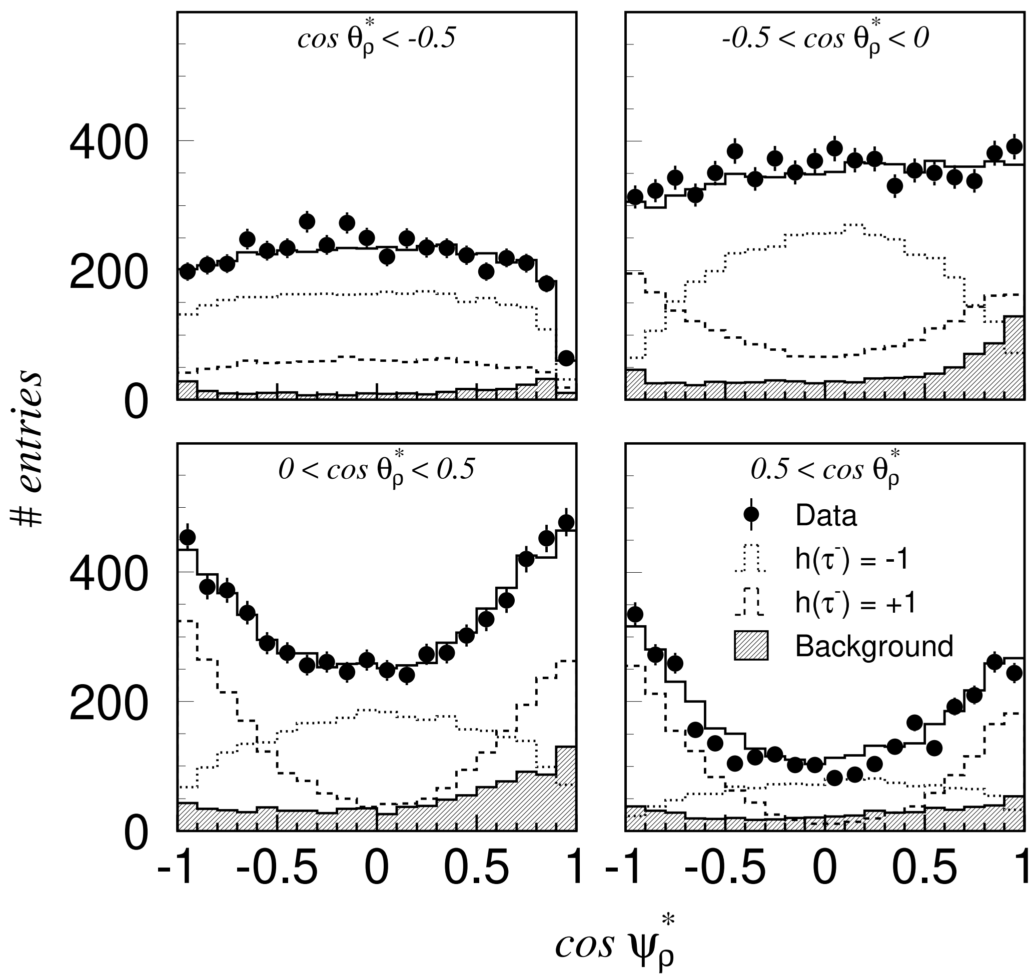

Figure 7: The angular distributions of the decays $\tau^- \to \rho^- \nu_\tau$ and $\rho^- \to \pi^- \pi^0$ with the result of the fit superimposed

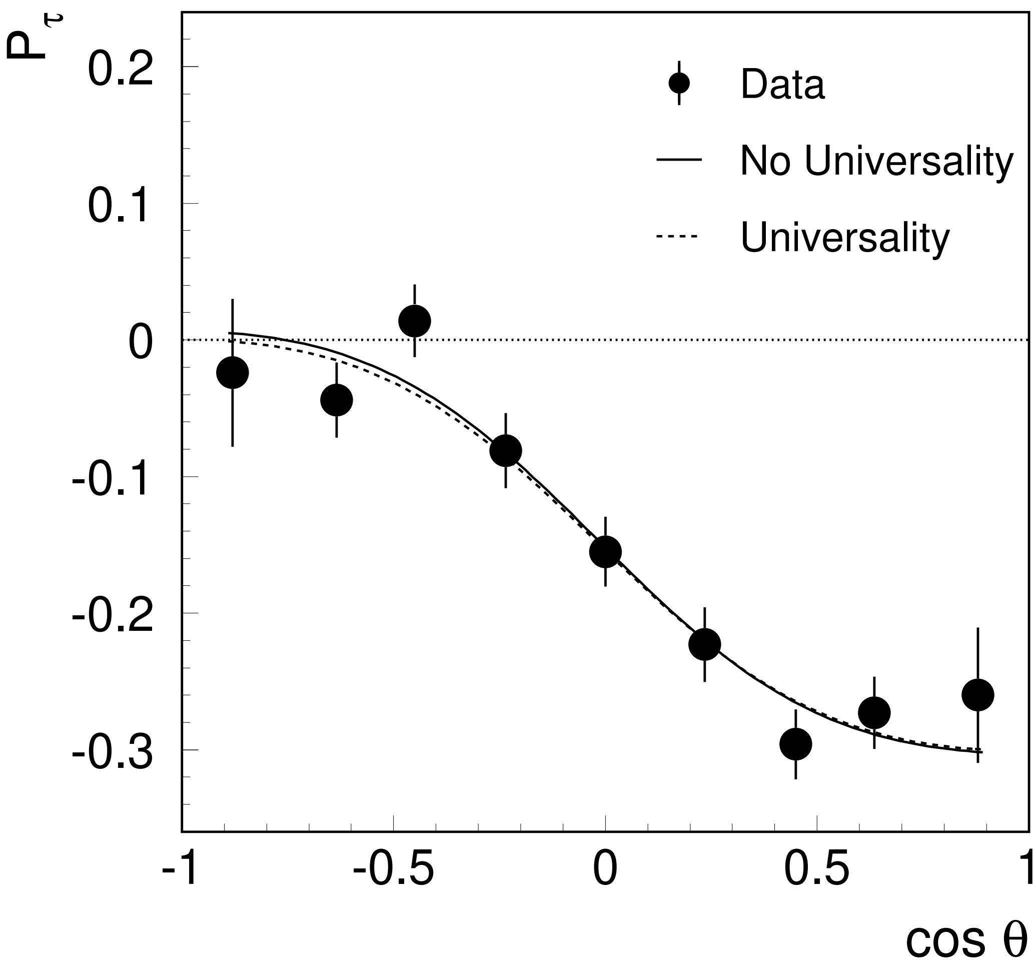

Figure 8: The polarisation $\mathcal{P}_\tau$ as a function of the scattering angle $\cos\theta$.

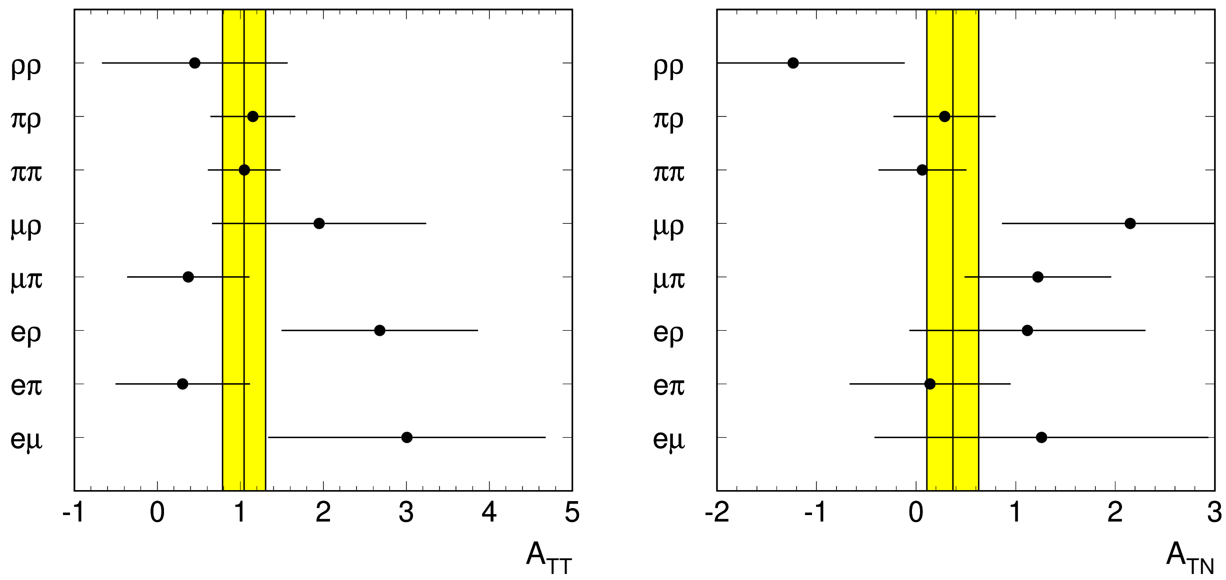

Figure 9: The results for $\mathcal{A}_{TT}$ and $\mathcal{A}_{TN}$. The error is statistical only. The χ^2/ndf for $\mathcal{A}_{TT}$ ($\mathcal{A}_{TN}$) is 5.8 / 7 (6.6 / 7) respectively. The solid line represents the fit result where the hatched area is the corresponding error.

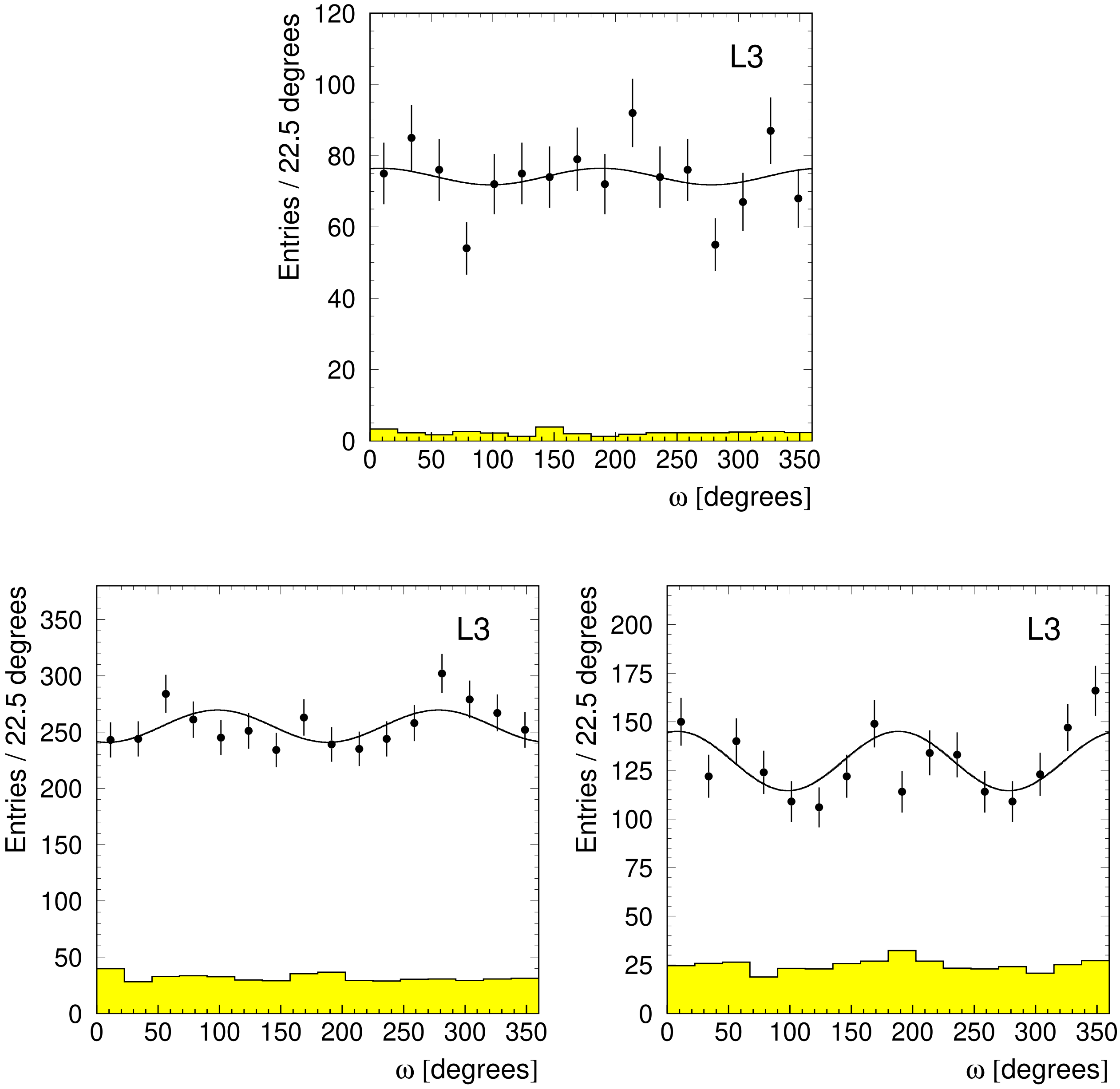

Figure 10: The ω distributions for the lepton-lepton final state (top), lepton-hadron final states (left) and hadron-hadron final states (right). The dots are data and the superimposed solid lines represent the results of this analysis. The total background contributions are shown in the hatched histograms.